J Appl Electrochem (2012) 42:233–248
DOI 10.1007/s10800-012-0389-1

ORIGINAL PAPER

Electrochemical investigations on the corrosion behavior and corrosion natural inhibition of API-X100 pipeline steel in acetic acid and chloride-containing CO_2-saturated media

Faysal Fayez Eliyan · Akram Alfantazi

Received: 28 November 2011 / Accepted: 6 February 2012 / Published online: 2 March 2012

Abstract The purpose of this experimental work was to investigate selected electrochemical aspects of the corrosion behavior of API-X100 in CO_2-saturated, multivariable-controlled corrosion media. Utilizing potentiodynamic polarization and electrochemical impedance spectroscopy (EIS), the corrosion rates, anodic dissolution, cathodic regimes, and free interfacial interactions were discussed. The tests were performed with respect to the environmental factors of 10, 20, 30, 40, 50, and 60 g L^{-1} chloride and of 10, 20, 30, 40, 50, and 60 mL L^{-1} acetic acid at 20 and 90 °C in the absence and presence of 10 vol% crude oil. The corrosion rates exhibited a peak value with respect to the chloride content while they increased continuously with the acetic acid content irrespectively from temperature. The corrosion behavior was nearly independent from chloride in the presence of acetic acid and oil demonstrated an effective inhibition in all conditions. EIS results showed an agreement with the polarization findings and indicated adsorption-controlled mechanisms.

Keywords Low alloy steel · EIS · Polarization · Kinetic parameters · API-X100 · Oil

1 Introduction

High strength low alloy (HSLA) pipeline steels have been recently considered for oil and gas transportation facilities by which an enhanced integrity is achieved. Although the extended allowance with respect to higher operation pressures and flow rates is then met with greater demand for energy resources, the associated time-dependent problems remain unresolved [1]. One of these problems is the chemical degradation caused by carbon dioxide accompanying the formation water which is intermixed with oil in the transported emulsions. Gaseous carbon dioxide dissolves in the formation water to produce the corrosive carbon-carrying species H_2CO_3 and HCO_3^- by which the corrosion reactions are driven. The severity of the corrosion attack, most commonly governed by the cathodic reactions [2] is dependent on the environmental factors, such as partial pressure of carbon dioxide (P_{CO_2}), temperature, pH, chloride content, and acetic acid [3]. In fact, the complexity of this type of corrosion arises from the inadequate understanding of the interrelation between these factors and on their consequent effect on the corrosion behavior, rate, and surface. Clover et al. [4] performed a high CO_2 pressure testing at 50 °C correlating the rate of localized and general corrosion attacks to the microstructures of several pipeline steels. The cathodic reactions were found proportional to the unassociated acetic acid and temperature in CO_2-saturated conditions of adjusted pH values of 4 showing corrosion penetration rates reaching 15 mm $year^{-1}$ [5]. In the context of the chemically multivariable-controlled corrosion, the acetic acid effect on the corrosion type was found temperature dependent and its "inhibitive" effect on the anodic reactions were limited by the chloride content [6]. Carbon dioxide corrosion in the multiphase environments can become a function of water content and/or dispersion in relation to the oil phase and, depending on the transportation velocity, corrosion rates can be effectively suppressed. Ajmera et al. [7] reported significant reductions in the corrosion rates in the CO_2-saturated solutions with respect to the effective chemical constituents in the crude oils correlating that to the wettability and hydrophilic and/or hydrophobic properties of the emulsified interfaces.

F. F. Eliyan (✉) · A. Alfantazi
The University of British Columbia, Vancouver, BC, Canada
e-mail: faysal09@interchange.ubc.ca

Paraffin-based crude oils were indicated as effective natural inhibitors decreasing the corrosion rates by as much as 50–70% at 42 °C during flow conditions attributing that to the polar nature of the adsorbed layers [8]. In the open literature, CO_2 corrosion did not receive a wide interest with respect to chemically multivariable-controlled mechanisms and the effect of natural inhibition in these conditions was not clearly elucidated from an electrochemical perspective.

In our work, a detailed electrochemical investigation was performed in unbuffered 1-bar-CO_2-saturated conditions with an extended range of chloride and acetic acid at 20 and 90 °C in the absence and presence of 10 vol% oil. Potentiodynamic polarization was utilized to study the effects of those two chemical factors in separate schemes and in an intermixed matrix of incremental amounts on the corrosion behavior. EIS was also employed to elucidate the electrochemical interactions at the interface considering the same environmental conditions. The electrochemical evaluations were carried out in a regular glass test cell setup to provide an understanding on corrosion and inhibition of a new generation pipeline steel API-X100.

2 Experimental details

2.1 Corrosion test setup

The tests were performed in a standard three-electrode glass jacket cell of a total volume of 1 L. The working electrode was made out of API-X100 pipeline steel, the counter electrode was a graphite rod, and the reference electrode was a saturated calomel electrode (SCE) of +0.241 V_{SHE} isolated at the laboratory ambient temperature. The electrochemical contact between the reference electrode and the working electrode was achieved by a Luggin capillary tube with a Vycor frit. The cell was connected to a Cole-Parmer heater controlled by a digital setup.

A gas bubbler was inserted into the cell to purge nitrogen gas for 120 min to deoxygenate the test solutions and then carbon dioxide was continuously purged throughout the test time periods. A gas mass-flow controller was used to control the flow rate of the purged gas to achieve an effective positive pressure inside the cell. The test solutions were continuously stirred by a magnetic stirrer to achieve an effective homogenous mixing when oil was introduced.

The three electrodes were connected to a Princeton Applied Research (PAR) Versastat 4 potentiostat/galvanostat whose functions are correlated to VersaStudio v1.50.3712 software program. Open circuit potentials (OCP), potentiodynamic polarization, and electrochemical impedance spectroscopy (EIS) test results were processed, analyzed, and presented to perform the electrochemical investigation with respect to the environmental factors.

2.2 Test material

The test samples were cut out of a pipeline segment made from API-X100 steel. They were machined into proper disks of nominal dimensions of a 15 mm diameter and 5 mm thickness and were soldered to copper wires by a conductive silver paste. Afterwards, they were mounted in special hard cold-curing epoxy resins. Prior to each corrosion test, they were sequentially wet ground by silicon carbide emery papers of 120, 320, and 600 grit. Afterwards, they were degreased ultrasonically with ethyl alcohol for 10 min and then rinsed with distilled water and dried in a cool air stream. The chemical composition analysis of the test material was made by inductive coupled plasma (ICP) and LECO carbon analysis techniques. The chemical composition on a weight percent basis is shown in Table 1. The optical microstructure of as-received steel is shown in Fig. 1. For the microstructural analysis, a sample was wet ground to 1,200 grit silicon carbide finish and then polished sequentially with 6 and 1 μm diamond suspensions. Afterwards, the sample was etched with 2% nital (2 mL acid + 98 mL ethyl alcohol) and then treated with alcohol swapping and dried in a cool air stream. The microstructure of the as-received sample showed a mixture of acicular ferrite and dispersed bainite colonies with micro-variations in color, possibly due to micro-variations in the alloying content.

2.3 Test solutions

The corrosion tests were performed in unbuffered 1-bar-CO_2-saturated media of sodium chloride with concentrations of 10, 20, 30, 40, 50 and 80 g L^{-1} and acetic acid of 10, 20, 30, 40, 50 and 80 mL L^{-1} prepared as oil-free solutions and 10 vol% oil-containing emulsions. The experiments were performed in unbuffered media with pH values between 4.2 and 4.8 in the acetic acid-free solutions and from 3.3 to 4 in the acetic acid-containing solutions

Table 1 The chemical composition and carbon equivalent of the steel used in this study

Composition (wt%)										CE
C	Mn	Mo	Ni	Al	Cu	Ti	Nb	Cr	V	
0.1	1.67	0.21	0.13	0.02	0.25	0.01	0.043	0.016	0.003	0.47

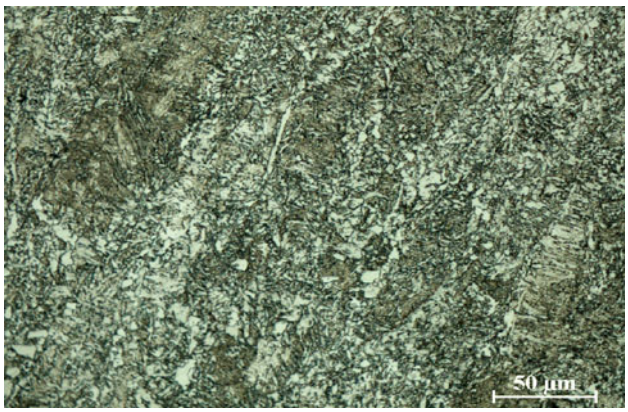

Fig. 1 Optical micrograph of API-X100 steel showing martensite (*dark*), bainite and ferrite (*light*) colonies

with respect to the chloride content and temperature. The relatively few amount of oil of 10 vol% was found not to affect the pH values. To achieve effective homogeneity between the aqueous brines and oil, dioctyl sulfosuccinate sodium ($C_{20}H_{37}NaO_7S$) salt, an anionic surfactant, was added with 0.2 wt% to the oil-containing emulsions. Table 2 shows selected properties of the emulsified hydrocarbon and, according to the crude oil classification based on the carbon number and density in [9], the test hydrocarbon represents a typical medium-weight crude oil. Double distilled deionized water was utilized for the test solutions and the salinity, and the acetic acid content ranges were extended to simulate some extremely corrosive saline stratum water cuts accompanying the decreasing oil content extracted from depleted oil wells [10]. The effect of temperature was set to be 20 and 90 °C within ±1 °C.

2.4 Electrochemical tests

After full deoxygenation and consequent CO_2 saturation were achieved at the required temperatures, the samples were immersed into the cell. Potentiodynamic polarization measurements were performed at a scan rate of 0.5 mV s^{-1} within a potential range at which the characteristic features of the anodic and cathodic regimes were fairly revealed with respect to the environmental factors. Electrochemical impedance spectroscopy (EIS) tests were performed to study the interfacial interactions during the open circuit potential. The frequency range was from 0.01 to 10,000 Hz with a sampling rate of 10 points per decade. The polarization tests were performed three times and the corrosion parameters of rate and potential exhibited a good reproducibility. EIS tests were performed at least three times showing reproducible impedance profiles of similar sizes and characteristics.

Table 2 Selected chemical and physical properties of the crude oil considered

Property	Details
Appearance	Pale yellow
Initial boiling point (°C)	170
Boiling range (°C)	170–390
Flash point (°C)	63
Lower/upper flammability (%V)	1–6
Auto-ignition temperature (°C)	>220
Vapor pressure (Pa)	<100 at 20 °C
Density (g cm^{-3})	0.84 at 15 °C
Kinematic viscosity (mm^2 s^{-1})	2–4.5 at 40 °C

3 Results and discussion

3.1 Potentiodynamic polarization tests

Potentiodynamic polarization tests were performed to study the corrosion behavior in oil-free and oil-containing conditions as illustrated in Figs. 2, 3, 4, 5, 6, 7, 8, 9, and 10 in which the amounts of acetic acid and chloride were varied from 10 to 60 mL L^{-1} and 10 to 60 g L^{-1}, respectively at 20 and 90 °C. The polarization behavior seemed to be governed by the cathodic capabilities of CH_3COOH, H_2CO_3, H^+, and H_2O, in which chloride also introduced significant changes in the cathodic regimes.

3.1.1 Oil-free test conditions

The corrosion behavior was first investigated in chloride-free conditions to reveal the cathodic effect on the accelerated corrosion reactions. The influence of the electroactive species involved in the polarization performance was segregated in acetic acid-free and acetic acid-containing, CO_2-saturated and N_2-saturated media, in four profiles shown in Fig. 2a. The least corrosion potential and rate resulted when the total reduction was exclusively dominated by H_2O and H^+. However, upon CO_2 saturation, the cathodic current densities were about an order of magnitude greater, revealing the substantially enhanced cathodic processes by H_2CO_3. This carbon-carrying agent is a consequence of CO_2 dissolution in water governed by dissociation equilibrium constants in low pH conditions of approximately 4. Therefore, the corrosion rate was higher accompanied by an expected more noble corrosion potential (E_{corr}) by as much as 45 mV. Interestingly, the anodic dissolution showed a continuous acceleration in comparison to that of N_2-saturated medium. This supports already proposed views on the possible direct involvement of H_2CO_3 and HCO_3^- in the dissolution mechanisms [11, 12] as follows:

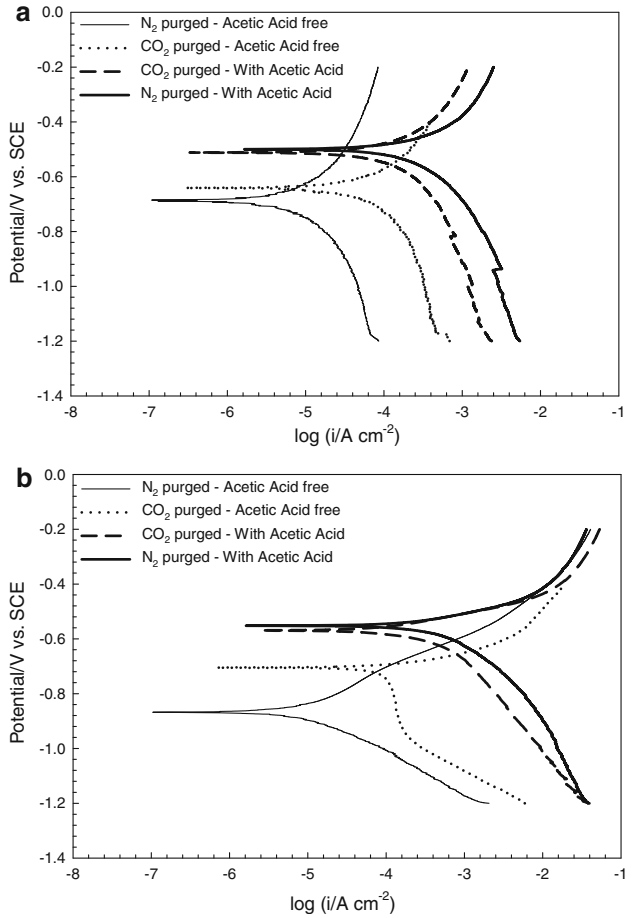

Fig. 2 Potentiodynamic polarization in CO_2-saturated and N_2-saturated conditions, free of and containing 10 mL L^{-1} acetic acid in **a** chloride-free and in **b** 10 g L^{-1} chloride-containing conditions

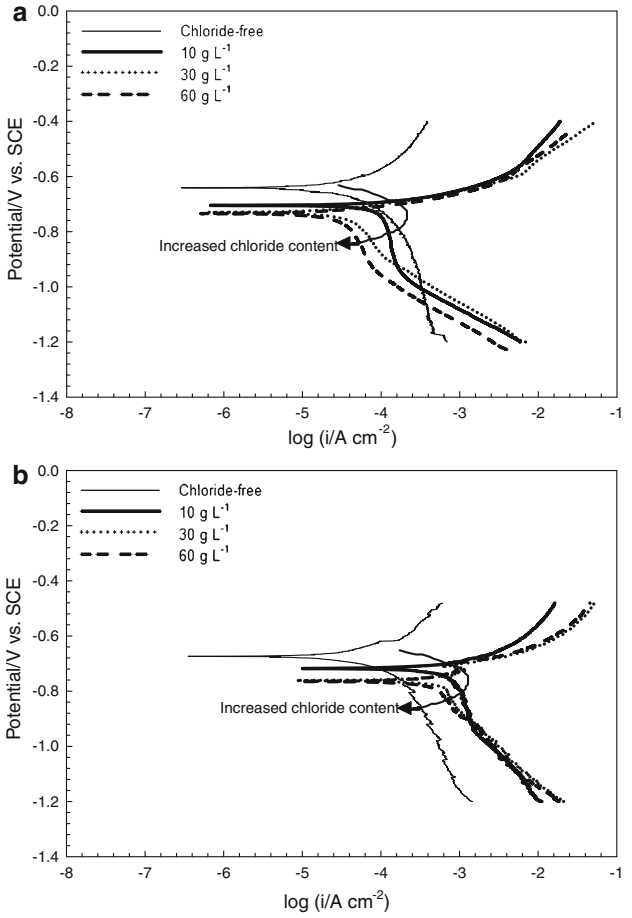

Fig. 3 Potentiodynamic polarization in oil-free, CO_2-saturated, chloride-free, and containing 10, 30, and 60 g L^{-1} chloride-containing conditions at **a** 20 and **b** 90 °C

$$Fe + H_2CO_3 \rightarrow FeCO_3 + 2H^+ + 2e^- \quad (1)$$

In addition $\left[FeHCO_3^+\right]_{ads}$ becomes involved in the dissolution mechanism as follows:

$$Fe + HCO_3^- \rightarrow FeHCO_3^+ + 2e^- \quad (2)$$

$$FeHCO_3^+ \leftrightarrow Fe^{2+} + HCO_3^- \quad (3)$$

The introduction of 10 mL L^{-1} of CH_3COOH nearly multiplied the cathodic regime covering that already resulted in the acetic acid-free-CO_2 saturated medium.

The corrosion rate consequently increased accompanied by enhanced CH_3COOH-influenced hydrogen evolution. Interestingly, the highest current densities were attained in the acetic acid-containing N_2-saturated medium, making the two extreme, maximum and minimum, corrosion rates and potentials in the N_2-saturated media.

There was a similar respect of corrosion exhibited in acetic acid-containing CO_2-saturated medium. However, the considerable deceleration in both anodic and cathodic branches in that condition suggests the ability of the active

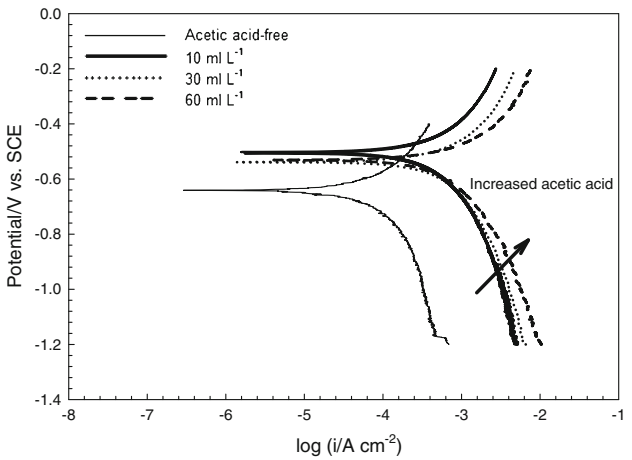

Fig. 4 Potentiodynamic polarization in oil-free, CO_2-saturated, acetic acid-free, and containing 10, 30, and 60 mL L^{-1} acetic acid-containing conditions at 20 °C

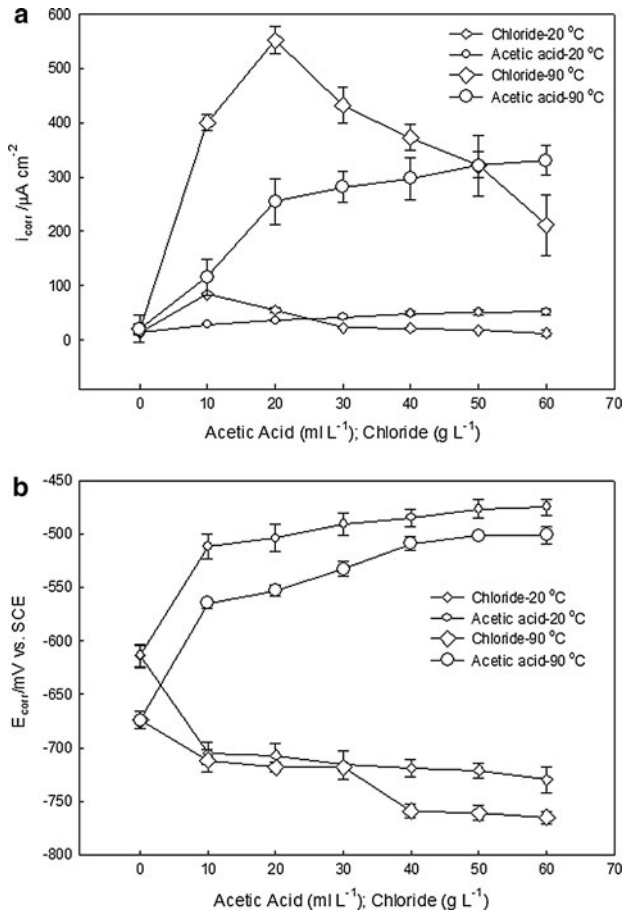

Fig. 5 **a** Corrosion current density and **b** corrosion potential variation with respect to chloride and acetic acid contents at 20 and 90 °C

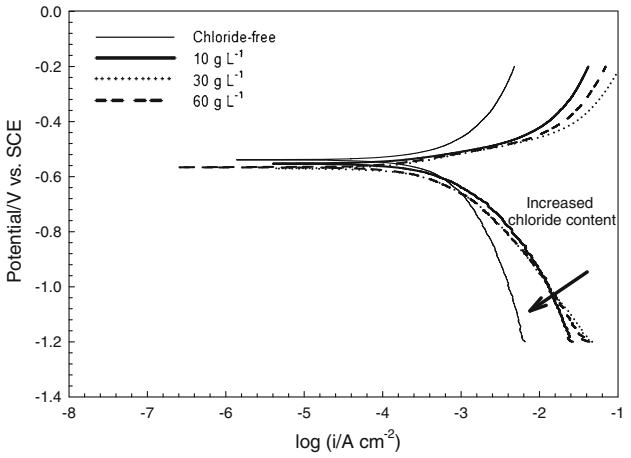

Fig. 6 Potentiodynamic polarization in oil-free, CO_2-saturated, acetic acid-free, and containing 10, 30, and 60 g L^{-1} in the presence of 10 mL L^{-1} acetic acid at 20 °C

carbon-carrying species in facilitating effective passivation even with the presence of acetic acid. Moreover, this might indicate that the cathodic reactions occurred, although in a decelerating manner, on these interfacial barriers or through impeded diffusion of the reducible species in possible mechanisms with respect to the salinity and acetic acid [13].

As shown in Fig. 2b, the same four cases were considered in the presence of 10 g L^{-1} chloride. In the case of acetic acid-free, N_2-saturated medium, the anodic reactions were greatly accelerated and E_{corr} was more negative accompanied by enhanced kinetics of water reduction. In addition, the active anodic polarization exhibited a multi-slope behavior corresponding possibly to an early formation of hydroxide-based films [14] before a continuous dissolution and/or transformation to stable oxide films as follows:

$$Fe + OH^- \leftrightarrow FeOH^-_{ads} \quad (4)$$

$$FeOH^-_{ads} \rightarrow FeOH_{ads} + e^- \quad (5)$$

$$FeOH_{ads} \rightarrow FeOH^+_{ads} + e^- \quad (6)$$

$$FeOH^+_{ads} + OH^- \rightarrow Fe(OH)_2 \rightarrow \text{Hydrous } [Fe(OH)_2] \quad (7)$$

However, in the CO_2-saturated medium, two distinct cathodic regimes were revealed. The corrosion behavior was anodically sensitive to chloride where the accelerated anodic polarization intersected the combined mass-limited cathodic reduction of H_2CO_3 and H^+. The active reductions of water in the acetic acid-free conditions were within nearly the same orders of magnitude and the corrosion rates were higher in comparison to the chloride-free conditions. The greatest cathodic current densities, with a modified mixed charge–mass transfer shoulder, were exhibited in N_2-saturated medium with the valid justifications proposed for the chloride-free conditions.

The investigations on the polarization behavior were further carried out to study the effect of chloride and acetic acid at separate schemes with specific ranges between 20 and 90 °C. As shown in Fig. 3a, comparative to the chloride-free condition at 20 °C, the behavior appeared to be anodically sensitive to the small dose of chloride of 10 g L^{-1} where the corrosion rate was as much as seven times higher and the corrosion potential was approximately 90 mV lower.

The cathodic regime exhibited the mass transfer limited reduction of H_2CO_3, and H^+ upon chloride-influenced kinetics of hydrogen evolution in the more conductive conditions of greater ionic strengths [15] similar to the observations reported in [16]. In addition, the reduction regime was finally dominated by purely charge-transfer reduction of water at similar potentials around –1 V_{SCE}, regardless of the chloride content. Corrosion current densities exhibited a "bow" on the Evan's map where the anodic sensitivity was restricted by decelerated cathodic reactions. The corrosion current densities showed a peak value before it decreased with the greater chloride content along with the steady decrease in the corrosion potentials. It seemed that the

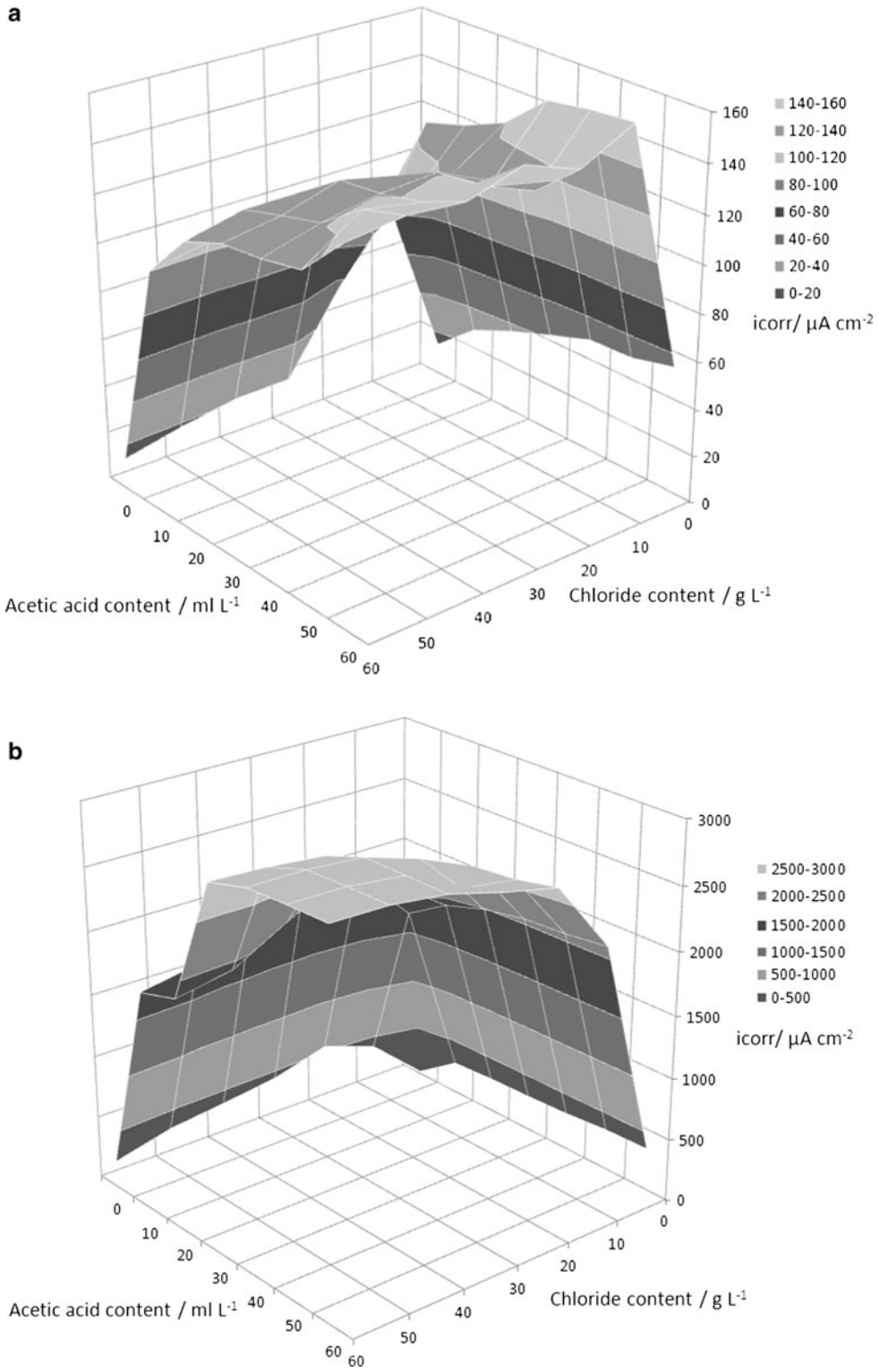

Fig. 7 3-D representation of corrosion current density variations with respect to chloride and acetic acid contents at **a** 20 and **b** 90 °C

corrosion behavior in chloride-containing CO_2-saturated media was associated with the physical changes at the corroding interfaces where the enhanced dissolution led to more effective supersaturation with the increased chloride content.

It seemed that the corrosion behavior in chloride-containing CO_2-saturated media was associated with the physical changes at the corroding interfaces where the enhanced dissolution led to more effective supersaturation with the increased chloride content. Chloride ions contributed in a

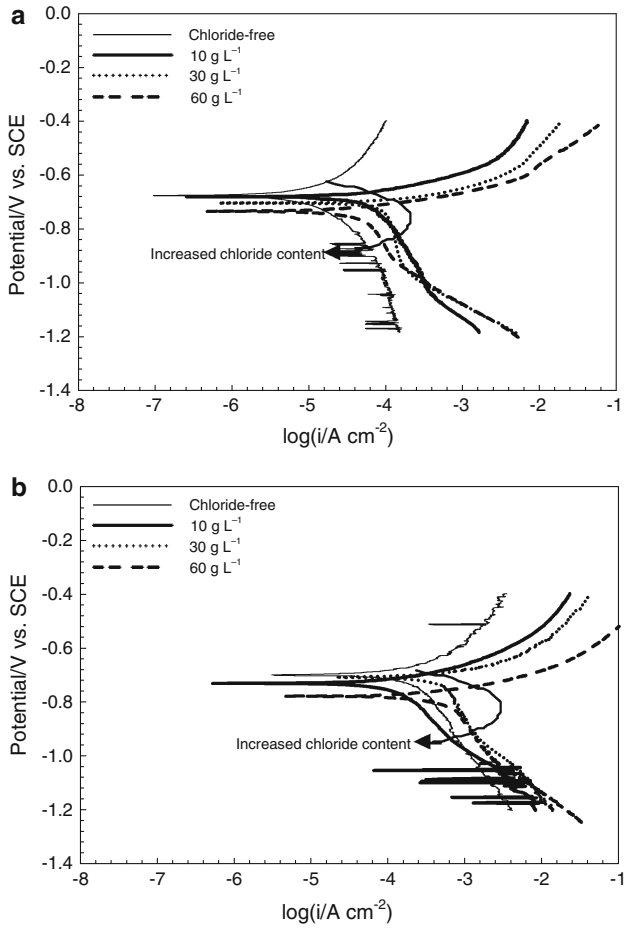

Fig. 8 Potentiodynamic polarization in oil-containing, CO_2-saturated, chloride-free, and containing 10, 30, and 60 g L^{-1} chloride at **a** 20 and **b** 90 °C

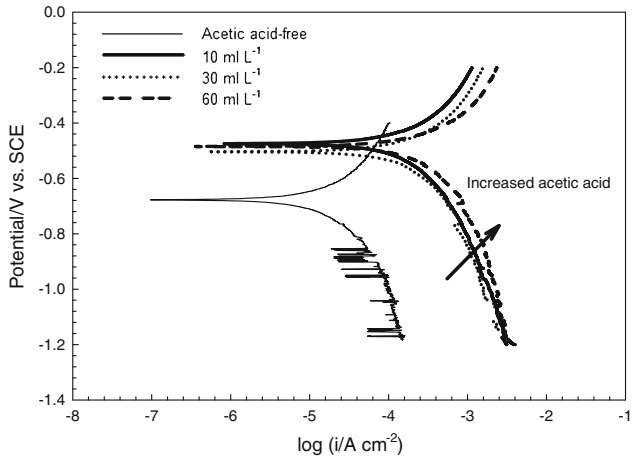

Fig. 9 Potentiodynamic polarization in oil containing, CO_2-saturated, acetic acid-free, and containing 10, 30, and 60 mL L^{-1} acetic acid at 20 °C

proportional manner in establishing pH gradients decreasing towards the corroding interfaces [17]. Ferrous ions (Fe^{2+}) consequently escaped from the conductive iron carbide

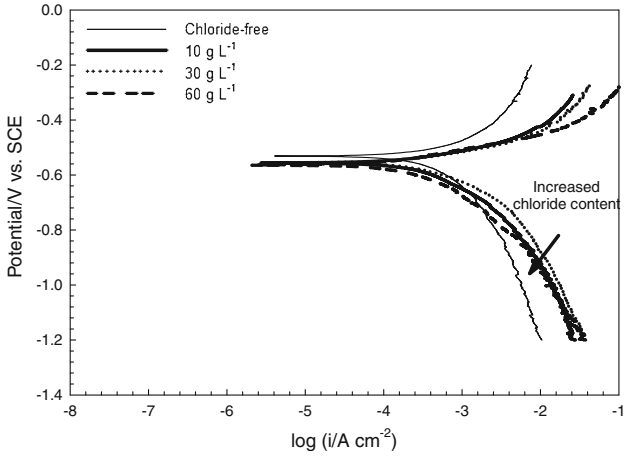

Fig. 10 Potentiodynamic polarization in oil-containing, CO_2-saturated, chloride-free, and containing 10, 30, and 60 g L^{-1} chloride in the presence of 10 mL L^{-1} acetic acid at 20 °C

(FeC_3) through which carbon-carrying species accumulated to combine with the increasing concentrations of Fe^{2+}. Iron carbonate ($FeCO_3$) precipitated over the FeC_3 leading to a deceleration in the cathodic reactions that confirms with the visual observations when the surfaces were more blackened during the cathodic phase right below the corrosion potentials when the amount of chloride was greater. At 90 °C, similarities to 20 °C conditions were exhibited, as shown in Fig. 3b, but with apparent accelerations in both anodic and cathodic branches. The cathodic reductions showed an extended kinetic regime making the total reduction of H^+ and/or H_2CO_3, existing with different speciation [18], more mixed charge–mass transfer controlled. The anodic dissolution in 50 and 60 g L^{-1} chloride conditions exhibited considerable retardations corresponding possibly to facilitated formation of more adherent corrosion products that could contribute to the active behavior.

The effect of acetic acid content from 10 to 60 mL L^{-1} was investigated at 20 °C from the polarization perspective in chloride-free conditions, which is shown in Fig. 4. Acetic acid reduction, described in Eq. 8 [19] prevailed the cathodic regime in these CO_2-saturated media, making the current densities multiplied by as much as five times higher.

$$2CH_3COOH_{(aq)} + 2e^- \rightarrow 2CH_3COO^-_{(aq)} + H_{2(g)} \quad (8)$$

Introduction of acetic acid increased the corrosion rates markedly, making the corrosion potentials as noble as 110 mV than that of acetic acid-free. 20 °C condition and the polarization behaviors at 90 °C were also similar. Corrosion current densities and corrosion potentials are collectively presented in Fig. 5a, b for acetic acid and chloride-containing conditions at 20 and 90 °C. The corrosion rates were significantly higher at 90 °C by as much as 17–20 times in chloride-containing solutions and by nearly 8 times in acetic acid-

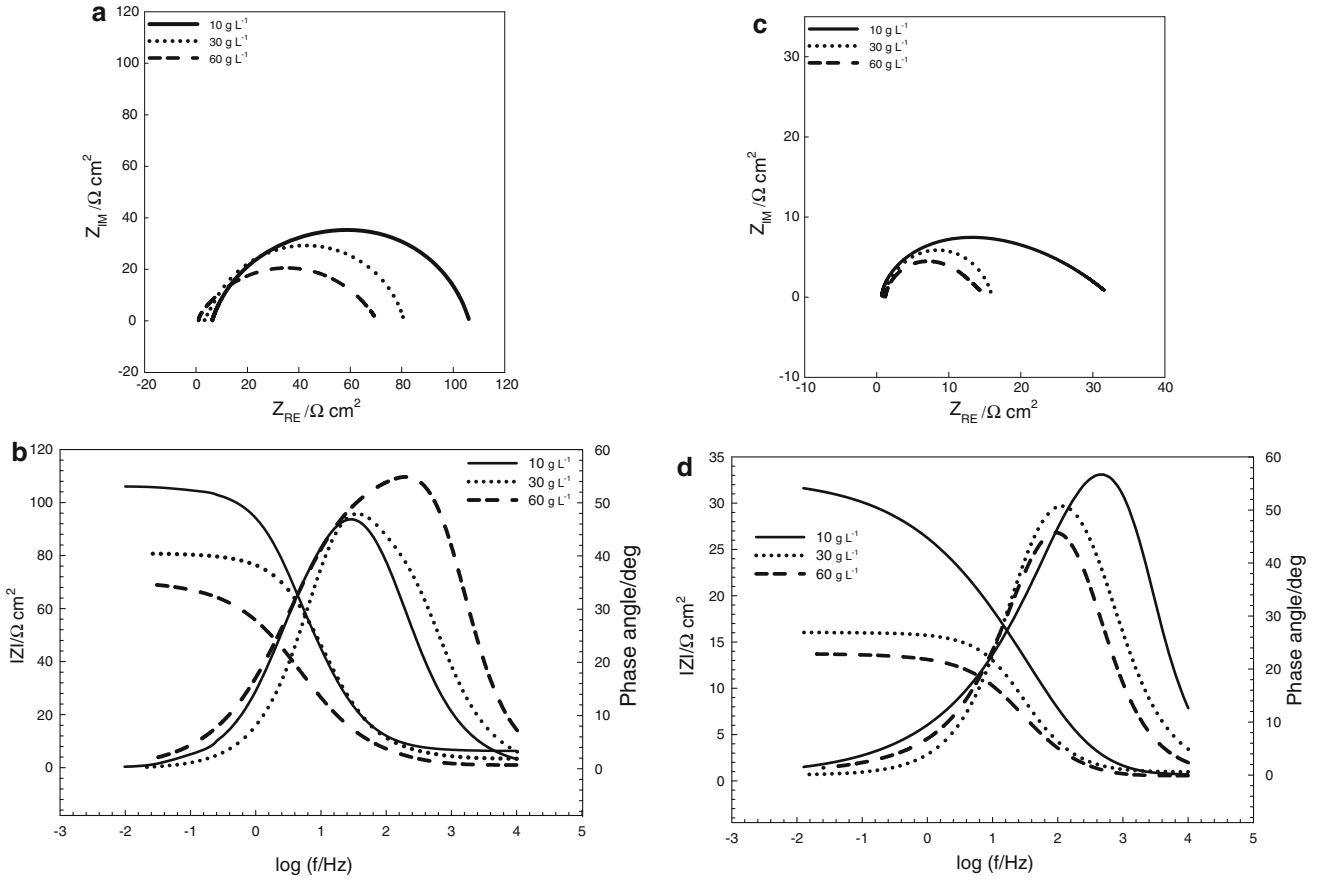

Fig. 11 Impedance of oil-free conditions with respect to the chloride content of 10, 30, and 60 g L^{-1} at 20 °C in **a** Nyquist and **b** bode; and at 90 °C in **c** Nyquist and **d** bode plots

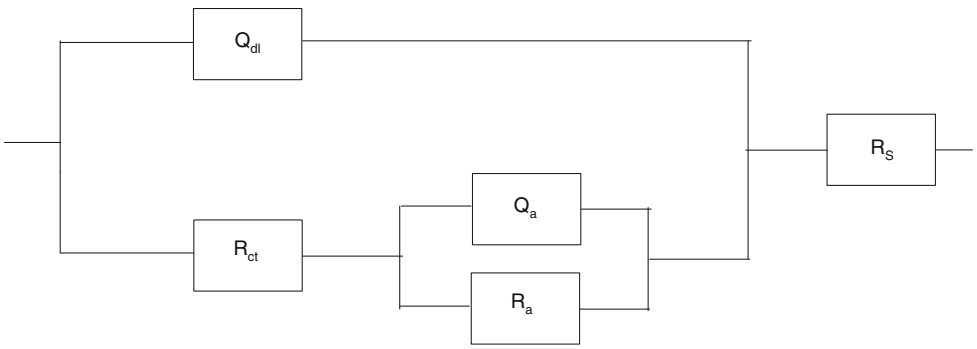

Fig. 12 Equivalent circuit proposed for the oil-free conditions at 20 and 90 °C

containing solutions. For the reasons discussed previously in this context, the corrosion rates were increasingly sensitive towards the few amounts of chloride before they showed peaks and consequently decreasing due to the decelerated cathodics. However, the corrosion rates were continuously proportional to the increased acetic acid content. It seemed also that the effect of chloride in increasing the corrosion rates was more significant than that of acetic acid at 90 °C. The corrosion potentials, as illustrated previously, increased with the acetic acid content and decreased with that of chloride in a steady manner. Interestingly, the higher temperature-accelerated anodic reactions made the corrosion potentials in both conditions lower.

The multi-variable-governed corrosion behavior was investigated on the basis of the effect of acetic acid on the variability of the corrosion rates with the increased chloride content. As shown in Fig. 6, the reduction of acetic acid, introduced with the amount of 10 mL L^{-1} prevailed the total cathodic reduction regimes along with the full range of chloride. The initial anodic sensitivity towards the chloride content was preserved, but the corrosion potentials were considerably higher than those in acetic acid-free conditions.

Table 3 Electrical component values of the equivalent circuit proposed for the oil-free conditions with respect to the chloride content at 20 and 90 °C

Temperature	Chloride content	Electric components							
(°C)	(g L^{-1})	R_s (Ω cm^2)	Q_{dl} (μF cm^{-2})	n_{dl}	R_{ct} (Ω cm^2)	Q_{ads} (μF cm^{-2})	n_{ads}	R_{ads} (Ω cm^2)	χ^2
20	10	6.73	18.4	0.621	87.46	26.7	0.987	12.56	2.4E−05
	30	3.63	31.2	0.842	10.00	25.0	0.818	62.63	1.5E−05
	60	1.00	48.2	0.916	4.63	20.7	0.627	70.28	4.5E−05
90	10	0.68	10.0	0.962	1.18	45.0	0.744	30.77	6.1E−05
	30	0.04	58.5	0.946	2.90	10.8	0.842	35.09	1.7E−05
	60	1.20	83.2	0.923	0.04	62.1	0.767	34.37	1.8E−05

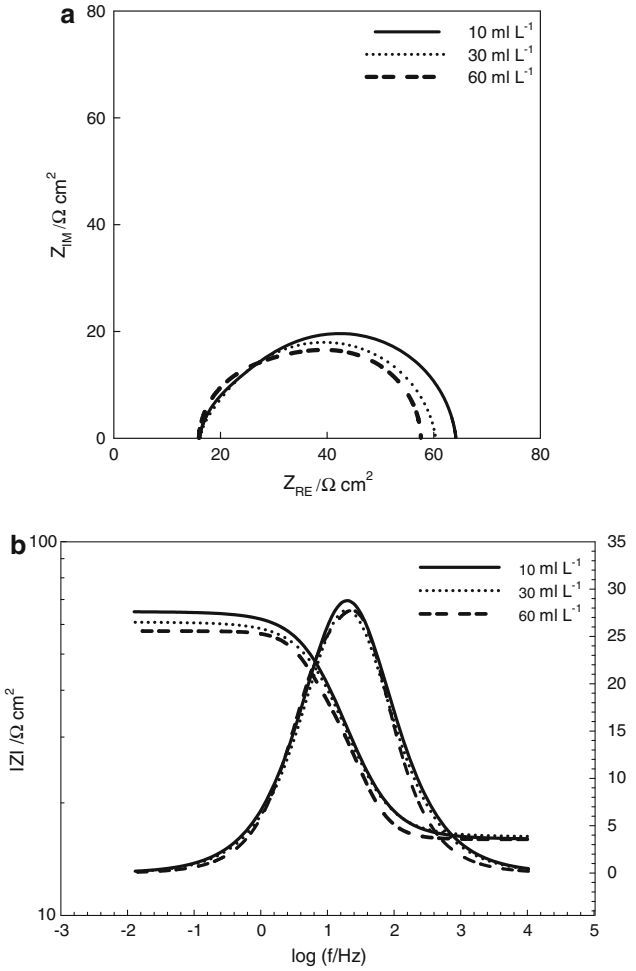

Fig. 13 Impedance of oil-free conditions with respect to acetic acid content of 10, 30, and 60 mL L^{-1} at 20 °C in **a** Nyquist and **b** bode plots

It seemed also that acetic acid, although it had greater corrosion rates in comparison to those of acetic acid-free conditions, made the corrosion rates independent from the chloride content. This could be due to the ability of acetic acid in interrupting the interfacial physical significance by which the variations of E_{corr}–i_{corr} were attributed to, when effective passivation had a strong tendency to form.

3-D comprehensive representations of the corrosion current density with respect to the chloride and acetic acid contents are shown for 20 and 90 °C, respectively in Fig. 7a, b. The corrosion rates were proportional to the acetic acid content in all chloride-containing solutions as if the elementary profile of acetic acid-free condition is exaggerated along with the acetic acid contents. Interestingly, the initial sensitivity towards the smallest chloride content producing a peak value was preserved and was increasing, as expected, with the greater acetic acid content. Acetic acid, introduced in different amounts, made the corrosion rates relatively independent from the greater chloride content. The corrosion rates seemed to be acetic acid controlled while in the most concentrated acetic acid-containing solutions, they showed elevated, yet fairly flat 3-D strip of corrosion rates. It is interesting that although there are similar trends that the corrosion rates exhibited with respect to acetic acid at the two chloride extremes, chloride-free and the most concentrated brines, the corrosion rates were nearly four times greater with the presence of chloride.

The corrosion rates at 90 °C were significantly greater and although the trends were appreciably similar with respect to the simultaneous effects of chloride and acetic acid, however, these effects seemed to be more identified. Except with the acetic acid-free, 10 and 20 mL L^{-1} containing conditions, the corrosion rates were proportional to the chloride content without exhibiting a significant peak. It appeared that there was a temperature-dependent acetic acid allowance for increased chloride contents to induce their full anodic effect where the corrosion rates increased without the retardation exhibited at 20 °C. In addition, the corrosion rates were progressively greater with the increased chloride and acetic acid contents in a manner not very discernable at 20 °C.

3.1.2 Oil-containing test conditions

The polarization behavior was investigated in 10 vol% oil-containing conditions considering the effect of chloride

Table 4 Electrical component values of the equivalent circuit proposed for the oil-free conditions with respect to acetic acid content at 20 and 90 °C

Temperature (°C)	HAc content (mL L^{-1})	Electric components							
		R_s (Ω cm^2)	Q_{dl} (μF cm^{-2})	n_{dl}	R_{ct} (Ω cm^2)	Q_{ads} (μF cm^{-2})	n_{ads}	R_{ads} (Ω cm^2)	χ^2
20	10	16.04	43.4	0.947	26.56	63.2	0.985	21.58	1.43E−05
	30	16.23	38.6	0.921	26.02	58.3	0.980	28.13	1.23E−05
	60	15.97	38.9	0.976	28.34	19.4	0.964	13.29	2.27E−05
90	10	0.89	60.3	0.613	0.02	76.8	0.982	1.55	2.32E−05
	30	0.46	67.0	0.645	0.41	19.6	0.988	0.55	6.39E−05
	60	0.92	72.3	0.688	0.25	50.9	0.971	2.80	6.99E−05

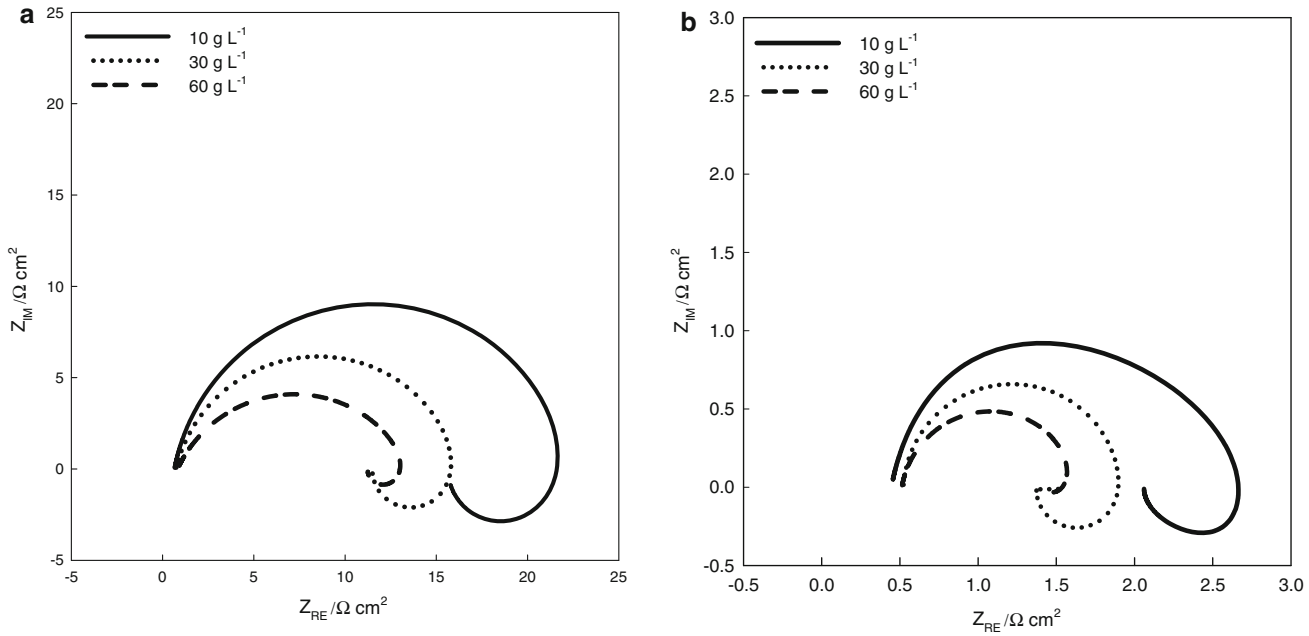

Fig. 14 Impedance of oil-free conditions with respect to chloride content of 10, 30, and 60 g L^{-1} in the presence of 20 mL L^{-1} acetic acid represented by Nyquist plots **a** 20 and **b** 90 °C

and that of acetic acid from preliminary perspectives without considering the extended simultaneous multi-variable effect. In the carbonated conditions, considering the variance of chloride, the corrosion rates decreased upon the addition of oil accompanied by a decrease in the corrosion potentials. In addition, although the trend exhibited in the polarization profiles in the oil-free conditions were persevered, however, the addition of oil made the chloride effect more pronounced; that is, the increased chloride content to the inhibited interfaces resulted in an enhanced cathodic effect and the corrosion potentials were more spaced, as shown in Fig. 8a at 20 °C. The relationship between oil miscibility and its adsorption capabilities for effective inhibition seemed to be apparent in the chloride-free and low chloride-containing conditions. As shown, the mass-limited cathodic regime in the chloride-free condition exhibited noise current spikes likely associated with the agglomerative interference of hydrogen evolution with the adsorbed hydrocarbon. Oil seemed also to modify the mass-limit reduction of H^+ and/or H_2CO_3 at potentials above -1 V_{SCE} to be mixed controlled with the charge transfer. This behavior could be subject for further investigations on the organic inhibitors effect on the reduction mechanisms with respect to chloride and/or carbon dioxide partial pressure. In the anodic regime, oil adsorption seemed involved in the pre-passivation phase to the extent that the effective, electrochemical-based, adsorption impeded the passivation process. This is suggested from the comparison with the oil-free conditions where the dissolution process seemed less retarded and, with respect to chloride, the anodic current densities were higher. At 90 °C, the current densities were nearly an order of magnitude greater and the dissolution kinetics was noticeably enhanced.

The corrosion potentials were kept within the same potential range of oil-free conditions although there was a slight decrease in corrosion rates and appreciable current noises in the cathodic regimes, as shown in Fig. 8b. In these conditions, oil was much less miscible resulting in compromised inhibition efficiency, but the nature of the cathodic inhibition seemed temperature independent.

The effect of oil on the corrosion behavior with respect to the increased acetic acid content was also investigated at 20 °C, as shown in Fig. 9. The corrosion rates were considerably less, but the influence of acetic acid reduction in elevating the corrosion potentials was preserved. In addition, the cathodic shoulders were modified with lower current densities and with appreciable noise in more separated mass-limited reduction profiles. The decelerated anodic current densities seemed to show earlier retardations, but still reflected the effect of increased acetic acid content. The behavior at 90 °C showed a similar behavior to that at 20 °C but with accelerated current densities. Oil seemed to enhance the effect of acetic acid in making the electrochemical response more independent from the chloride content, as shown in Fig. 10. Although there was a decrease in the corrosion rates, the presence of 10 mL L^{-1} acetic acid resulted in similar corrosion behaviors with respect to the absence and/or presence of chloride.

3.2 Electrochemical impedance spectroscopy (EIS)

The electrochemical interactions were studied by electrochemical impedance spectroscopy (EIS) to elucidate the possible mechanism(s) and the interrelated chemical contributions of acetic acid and chloride at the corroding interfaces. Within a specific range of frequency at open circuit potentials (OCP) and potentiostatic conditions, the impedance response was characterized with equivalent circuits of proper electrical elements [20]. The same range of acetic acid and chloride in the polarization tests were considered at 20 and 90 °C in oil-free and oil-containing CO_2-saturated emulsions.

3.2.1 Oil-free test solutions

Nyquist plots representing the oil-free conditions with respect to the chloride content at 20 and 90 °C are shown in Fig. 11. Nyquist profiles depicted similar mechanisms as the complex plane features across the frequency range at both temperatures showed a similarity. Partially depressed semicircles were exhibited proportionally decreasing with the chloride content with variations at low frequency where the significance of possibly cathodic charge-transfer processes appears [21]. At the interface, the corrosion is governed by two simultaneous processes interchangeably influencing dissolution and other physically developed factors [22, 23]: kinetics and adsorption. In CO_2-saturated media, the cathodic reactions govern the corrosion problem [24] where the hydrogen generation is driven by the carbon-carrying species being dominantly reduced in charge-transfer fashion. Over time, adsorption of the electroactive species becomes the rate determining step [25]. Therefore, in our case during the free conditions, adsorption resulted in depressed semicircles extending in some cases to reveal a relative overlapping between the medium and low frequency regions. The increased amount of chloride activated the corroding ferrite colonies, and, in turn, became less polarization resistant, which confirms with polarization results. The capacitive nature exhibited, regardless of the environmental factors of chloride and temperature, is associated with the presence of the enhanced cathodic platform of iron carbide (FeC_3) [26]. This layer possibly became an active conductive part of the microstructure of our high strength steel of 0.47 wt% C. The cathodic reactions accelerated by the chloride-sensitive localized pH gradients across the porous FeC_3 lead to increased, kinetically dependent, dissolution and resulted in single bode phase peaks within almost the same order of magnitude. At 20 °C, phase peaks exhibited a gradual increase with the chloride content reflecting the enhanced electrochemical role of processes outside the double layer. In 60 g L^{-1} chloride-containing condition, the peak was broader and the bode behavior changed in the medium to low frequency region, suggesting a possible onset change in the governing mechanism. This could be attributed to an initiated formation of a mixed layer of $FeCO_3$ and FeC_3 where the supersaturation possibly increased with the already plentiful amounts of the reducible species. At 90 °C, the Nyquist plots decreased in size as adsorption became more significant and the phase peaks showed a shift to higher frequencies, but were comparable. The proposed equivalent circuit of the configuration $\{R(Q(R(QR)))\}$ achieved a perfect fitting with the experimental data and is shown in Fig. 12. Solution resistance and resistances at the double layer and across the adsorption fields are represented by R_s, R_{ct}, and R_{ads} respectively. Although the capacitance and/or pseudo capacitance was exhibited, a constant phase element (CPE) was considered to account for the surface heterogeneities at the double layer (Q_{dl}) and the adsorption field (Q_{ads}). The CPE impedance (Z_{CPE}) is described by Eq. 9 as follows [27]:

$$Z_{CPE} = 1/Q(j\omega)^n \tag{9}$$

ω is $2\pi f$, j equals $\sqrt{-1}$, and n is a factor which has a value between 0 and 1. As shown in Table 3, R_s decreased with the increased chloride content and higher temperature and, as a result of the enhanced dissolution charge transfer, showed a continuous decrease. Interestingly, Q_{dl} showed an opposite trend as it seemed proportional with the

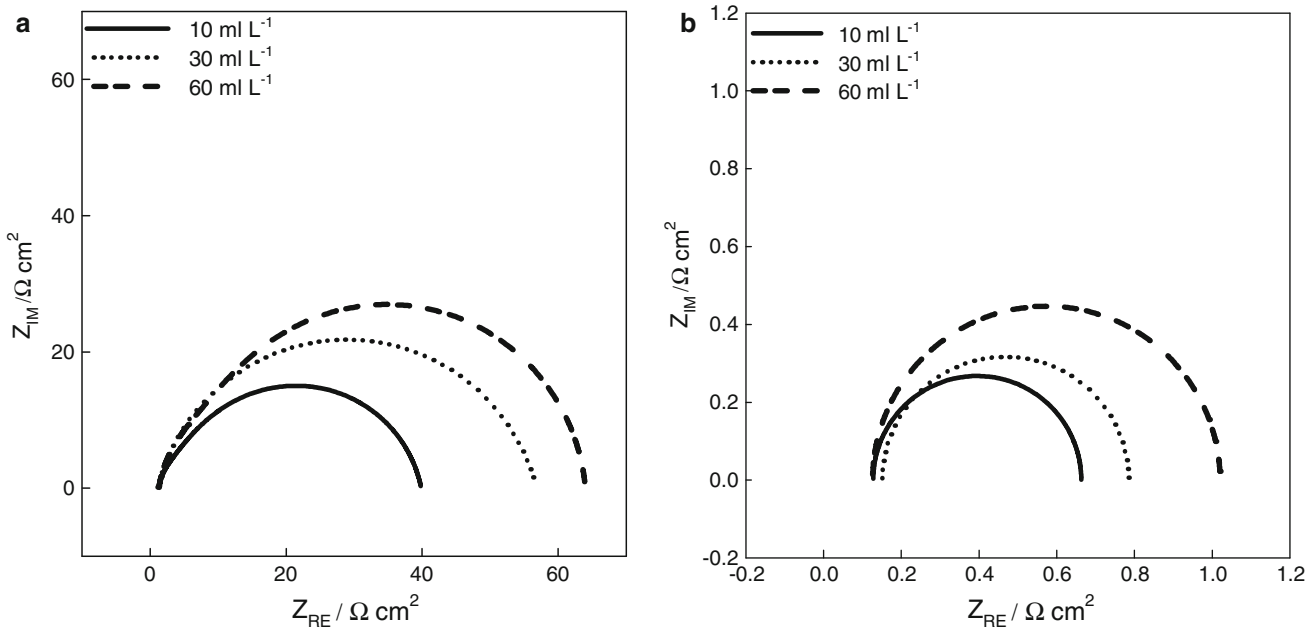

Fig. 15 Impedance of oil-free conditions with respect to acetic acid content of 10, 30, and 60 mL L^{-1} in the presence of 30 g L^{-1} chloride represented by Nyquist plots **a** 20 and **b** 90 °C

conductive platform developed for hydrogen evolution [28]. Adsorption resistance at 20 °C was proportional to the chloride content where adsorption became more pronounced on active areas possibly covered by more intermediate species [29]. χ^2 values are included in the same table and indicate the perfect fitting with orders of 10^{-5}. At 90 °C, charge transfer was significantly less across capacitive fields and adsorption resistance showed a relative independence from chloride content.

Introduction of acetic acid enhanced the cathodic power of the already corrosive CO_2-saturated media which is indicated by Eq. 8 where dissolution was accelerated. As shown in Fig. 13, for 20 °C conditions, the Nyquist loops were more capacitive, decreasing in proportion with acetic acid amount. The almost perfect semicircles were smaller than those exhibited with respect to the chloride content confirming with the polarization tests results as less polarization resistance is depicted. Therefore, the accelerated cathodic kinetics resulted in single peaks at comparable phase angles and low frequencies. Impedance moduli |Z| were relatively close to each other at both the high and low frequency regions. The impedance response at 90 °C was similar, reflecting a temperature-independent charge-transfer dominated mechanism, but with enhanced dissolution of smaller semicircles. The equivalent circuit proposed for the chloride-containing conditions achieved a reliable fitting to the impedance data of acetic acid conditions, and the electric components are shown in Table 4. Solution resistance values were higher than those in chloride-containing conditions and were comparable in acetic acid content at both temperatures. Charge transfer resistance, as well as that of adsorption, were almost independent from the content, but showed a great dependence on temperature across the more capacitive regions characterized. The compliance of the proposed mechanism for acetic acid-containing conditions were achieved, regardless of both content and temperature, which is different from the results indicated for the low frequency loops in [30]. This could be attributed to the chemical factors induced by the presence of approximately 80 g L^{-1} NaCl and other varying amounts of $CaCl_2$ and $MgCl_2{\cdot}6H_2O$ considered in the simulated oil field formation water in the study.

Introduction of acetic acid with an amount of 20 mL L^{-1} changed the interfacial influence of by-amount chloride. As shown in Fig. 14, the Nyquist plots representing the interrelated interaction of chloride and acetic acid at 20 and 90 °C resulted in depressed capacitive high-frequency semicircles and inductive low frequency loops. Acetic acid made the adsorption process slower as it was more favorable on the conductive FeC_3 in the acetic acid-free conditions. As a result, chloride preserved its proportional role in decreasing the polarization resistance in conditions where the cathodic reactions became accelerated and dominantly controlled by charge transfer, similar to the results in [30]. At 90 °C, the mechanism was similar with respect to the chloride content but the complex impedance was nearly an order of magnitude smaller than at 20 °C.

The interaction between chloride and acetic acid was studied from a different perspective where the interfacial

effect of acetic acid is considered in the presence of 30 g L^{-1} chloride as shown in Figs 15a, b at 20 and 90 °C, respectively. Although the basic adsorption-governed mechanism did not show a change in comparison to the chloride-free conditions, the increased acetic acid content induced an adverse effect on the polarization resistance [31]. The overlapped low frequency loop increased in size accordingly where the enhanced cathodic reactions seemed to be counterpart by effective precipitation of $FeCO_3$. At the interface, $FeCO_3$ became incorporated with the porous iron carbide blocking the active sites as already indicated in [32] where the introduction of acetic acid caused a temporary increase in the corrosion rates, but $FeCO_3$ showed morphological changes and remained protective.

3.2.2 *Oil-containing test solutions*

Nyquist and bode impedance representations for oil-containing conditions at 20 and 90 °C are shown collectively in Fig. 16 with respect to the chloride content. Oil inhibited the active interfaces more significantly in lower chloride-containing emulsions. The high-frequency semicircles were substantially depressed followed by inductive loops resulting from the adsorbed oil layers similar to the results reported in [33]. The significance of increased chloride content on decreasing the polarization resistance was exhibited in the low frequency regions. Oil induced interfacial changes throughout the frequency range were comparative with the oil-free conditions, as revealed from the bode plots. The broader phase peaks showed a slight shift to higher frequencies and showed a valley within comparable low frequencies as a signature of effective induction. Different from the results in [34] on the imidazoline-based inhibition performance, the bode profiles did not show multi slopes at low frequencies, excluding the hypothesis of multitime-constant inhibition impedance.

At 90 °C, the significance of oil adsorption was less confirming with the visual observation of less oil miscibility at higher temperatures. Nevertheless, inductive impedance was exhibited in the concentrated chloride

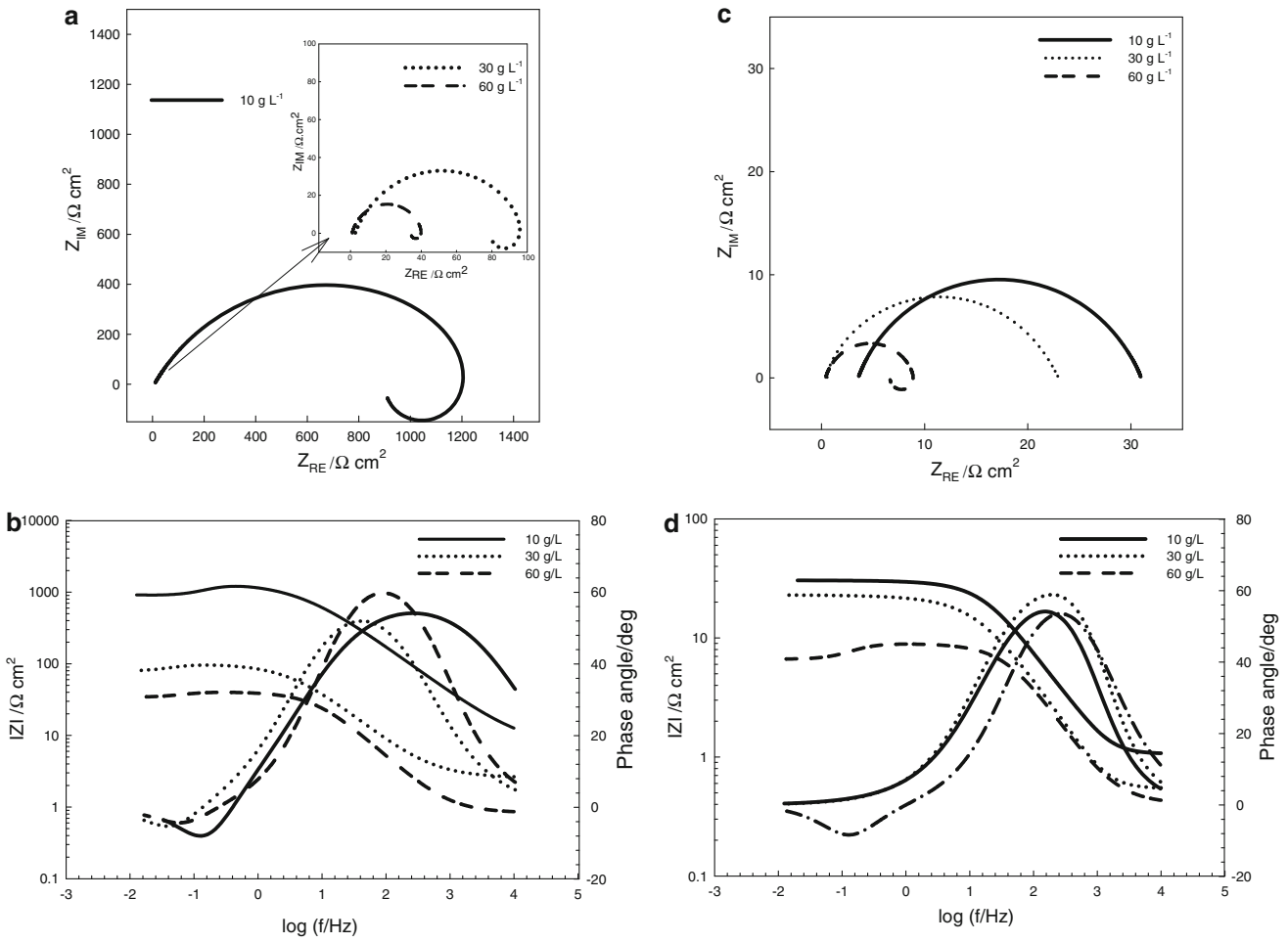

Fig. 16 Impedance of oil-containing conditions with respect to the chloride content of 10, 30, and 60 g L^{-1} at 20 °C in **a** Nyquist and **b** bode; and at 90 °C in **c** Nyquist and **d** bode plots

Table 5 Electrical component values of the equivalent circuit proposed for the oil-containing conditions with respect to the chloride content at 20 and 90 °C

Temperature (°C)	Chloride content (g L^{-1})	Elements							
		R_s (Ω cm^2)	Q_{dl} (μF cm^{-2})	n_{dl}	R_{ct} (Ω cm^2)	R_L (Ω cm^2)	L (H cm^{-2})	χ^2
20	10	6.74	71.4	0.677	900.21	458.8	377.6	4.1E−05
	30	2.55	92.6	0.753	76.78	21.61	68.4	5.3E−05
	60	0.83	99.4	0.833	33.32	6.716	15.2	5.5E−05
Temperature (°C)	Chloride content (g L^{-1})	Elements							
		R_s (Ω cm^2)	Q_{dl} (μF cm^{-2})	n_{dl}	R_{ct} (Ω cm^2)	Q_{ads} (μF cm^{-2})	n_{ads}	R_{ads} (Ω cm^2)	χ^2
90	10	3.550	11.6	0.776	25.96	48.1	0.776	1.542	3.4 E–05
	40	0.546	25.5	0.971	3.46	21.18	0.668	18.990	3.6 E–05
Temperature (°C)	Chloride content (g L^{-1})	Elements							
		R_s (Ω cm^2)	Q_{dl} (μF cm^{-2})	n_{dl}	R_{ct} (Ω cm^2)	R_L (Ω cm^2)	L (H cm^{-2})	χ^2	
90	50	0.402	10.71	0.845	6.937	2.378	2.38	4.4E−05	
	60	0.704	12.69	0.833	6.176	3.497	3.09	3.8E−05	

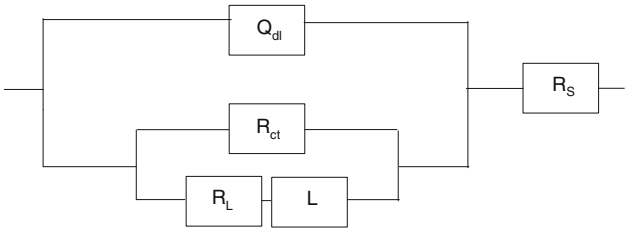

Fig. 17 Equivalent circuit proposed for the oil-containing conditions at 20 and 90 °C

emulsions of 50 and 60 g L^{-1} at which the extent of interaction between oil and the adsorbed electroactive species was not clear. As shown in Table 5, charge-transfer resistance was nearly an order of magnitude greater than that of oil-free conditions at 20 °C as Q_{dl} showed an opposite trend with a capacitive character with respect to the chloride content. As expected, the significance of oil adsorption was less with the increased chloride content, as depicted from trends of the induction parameters R_L and L. The equivalent circuit proposed for the oil-influenced induction is shown in Fig. 17 and achieved a perfect fitting with the experimental data. The Nyquist profiles with respect to acetic acid in oil-containing conditions are shown in Fig. 18, showing the similar significance of oil inhibition exhibited in chloride-containing conditions. However, oil did not cause a significant reduction in the charge transfer, as indicated by the trends of R_{ct} and R_L that are shown in Table 6 where the enhanced cathodic generation of hydrogen destabilized the oil layers.

4 Conclusion

In this experimental work, the electrochemical evaluation of API-X100 pipeline steel revealed important information about the multichemical effects on the corrosion behavior in CO_2-saturated media. It was useful to study the interactions between chloride and acetic acid when introduced with different amounts and it was confirmed that acetic acid effect prevailed that of chloride. Acetic acid made the corrosion behavior almost independent from the chloride content in a manner proportional with its content and when the temperature was higher. The basic findings can be summarized as follows:

1. The lowest corrosion current densities and corrosion potentials were in the acetic acid-free, N_2-saturated conditions regardless of chloride content. The introduction of acetic acid enhanced the cathodic reactions, but chloride enhanced the kinetics of water reduction. In addition, it was evident that there was a direct

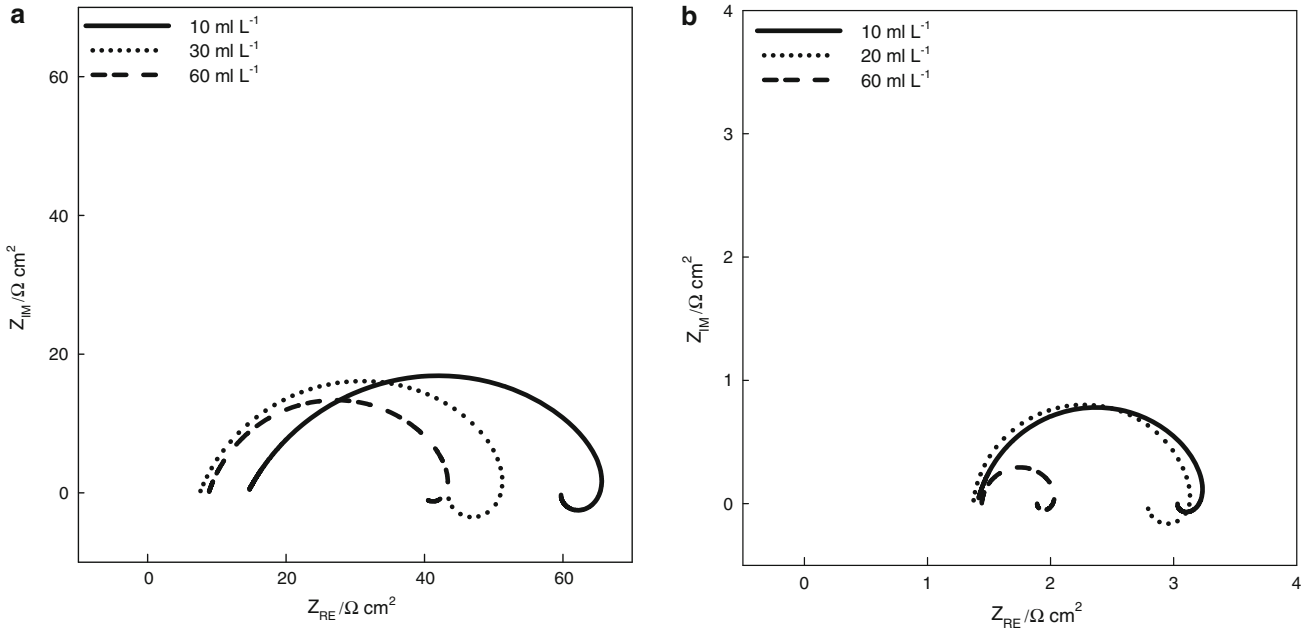

Fig. 18 Impedance of oil-containing conditions with respect to acetic acid content of 10, 30, and 60 mL L^{-1} represented by Nyquist plots **a** 20 and **b** 90 °C

Table 6 Electrical component values of the equivalent circuit proposed for the oil-containing conditions with respect to acetic acid content at 20 and 90 °C

Temperature (°C)	Chloride content (g L^{-1})	Electric components						
		R_s (Ω cm^2)	Q_{dl} (μF cm^{-2})	n_{dl}	R_{ct} (Ω cm^2)	R_L (Ω cm^2)	L (H cm^{-2})	χ^2
20	10	14.54	83.1	0.697	45.40	10.07	5.43	3.6E−05
	30	7.54	78.6	0.763	35.94	11.31	4.81	1.4E−05
	60	8.83	88.1	0.801	31.13	5.59	2.35	1.6E−05
90	10	1.40	14.8	0.864	1.62	5.31	0.0074	2.3E−05
	30	1.42	65.6	0.509	1.25	0.97	0.0116	1.3E−05
	60	1.44	71.4	0.961	0.45	0.178	0.0063	2.9E−05

involvement of carbon-carrying species in the anodic dissolution mechanisms.

2. Anodic sensitivity towards chloride was limited by decelerated cathodic reactions while the corrosion rates were proportional to the acetic acid content with more noble corrosion potentials. The corrosion potentials decreased with the chloride content and at higher temperatures.
3. The corrosion rates increased with increased chloride and acetic acid content while the corrosion behaviors became nearly independent from the chloride content in the presence of acetic acid at both temperatures.
4. Oil caused a significant deceleration in current densities but with a greater effectiveness at low temperatures and in the acetic acid-free conditions.
5. EIS results showed an agreement with the polarization data reflecting the significance of adsorption of the intermediate species in both chloride-containing and acetic acid-containing conditions. However, the interfacial interactions became inductive with respect to the chloride content in the presence of acetic acid and the effect of acetic acid on the polarization resistance changed in the presence of chloride.
6. Regardless of temperature, oil adsorption made the Nyquist profiles larger exhibiting induction loops. The profiles varied in the same respect towards the environmental factors in the oil-free conditions.

Acknowledgments The authors would like to thank Qatar National Research Fund (QNRF) for providing the financial support for this work.

References

1. Kermani M, Morshed A (2003) Corrosion 59:659
2. Lopez D, Perez T, Simison S (2003) Mater Design 24:561
3. Murata T, Sato E, Matsuhashi R (1986) Factors controlling corrosion of steels in CO_2-saturated environments. CORROSION/1986, Paper no. 7, NACE
4. Clover D, Kinsella B, Pejcic B, De Marco R (2005) J Appl Electrochem 35:139
5. George K, Nesic S (2007) Corrosion 63:178
6. Gulbrandsen E, Bilkova K (2006) Solution chemistry effects on corrosion of carbon steels in presence of CO_2 and acetic acid. CORROSION/2006, Paper no. 364, NACE
7. Ajmera P, Robbins W, Richter S, Nesic S (2010) The role of asphaltenes in inhibiting corrosion and altering the wettability of the steel surface. CORROSION/2010, Paper no. 329, NACE
8. Morales J, Perdomo J, Ramirez M, Viloria A (2000) Effect of crude oil contaminants on the internal corrosion in gas pipelines. CORROSION/2000, Paper no. 40, NACE
9. Lyons W, Plisga G (2005) Standard handbook of petroleum and natural gas engineering. Elsevier Inc, UK, pp 2–107
10. Mullins O (2008) The physics of reservoir fluids: discovery through downhole fluid analysis. Schlumberger, USA, p 144
11. Moiseeva L, Kuksina O (2003) Prot Met 39:490
12. Hirnyi S (2001) Mater Sci 37:491
13. Okafor P, Nesic S (2007) Chem Eng Commun 194:141
14. Castro E, Vilche J (1991) J Appl Electrochem 21:543
15. Fartash R, NavabZadeh S, Amirkhizi H (2010) Asystematic approach toward selection of cost-effective and corrosion resistant materials and corrosion inhibition and protection methods by using corrosion prediction models. CORROSION/2010, Paper no. 368, NACE
16. Fang H, Brown B, Nesic S (2010) High salt concentration effects on CO_2 corrosion and H_2S corrosion. CORROSION/2010, Paper no. 276, NACE
17. Makar G, Tromans D (1996) Corrosion 52:250
18. Takenouchi S, Kennedy G (1965) Am J Sci 263:445
19. Singer M, Brown B, Camacho A, Nesic S (2007) Combined effect of CO_2, H_2S and acetic acid on bottom of the line corrosion. CORROSION/2007, Paper no. 661, NACE
20. Cottis R, Turgoose S (1999) Electrochemical impedance and noise. NACE International, USA, p 9
21. Nesic S, Postlethwaite J, Olsen S (1996) Corrosion 52:280
22. Chen Y, Jepson W (1999) Electrochim Acta 44:4453
23. Fan X, Liu W, Cai F, Guo H, Wu Y, Du Q, Lu M (2011) Electrochemical characterization of erosion–corrosion of X70 pipeline steel under jet impingement conditions. CORROSION/2011, Paper no. 241, NACE
24. Remita E, Tribollet B, Sutter E, Vivier V, Ropital F, Kittel J (2008) Corros Sci 50:1433
25. Farelas F, Galicia M, Brown B, Nesic S (2010) Corros Sci 52:509
26. Laethaison N (2011) Carbide formation on carbon steels in CO_2 corrosion by use of applied anodic current. Master's thesis, University of Stavanger
27. Jorcin J, Orazemb M, Pebere N, Tribollet B (2006) Electrochim Acta 51:1473
28. López D, Schreiner W, de Sánchez S, Simison S (2003) Appl Surf Sci 207:69
29. Li P, Tan T, Lee J (1996) Corros Sci 38:1935
30. Zhu S, Fu A, Miao J, Yin Z, Zhou G, We J (2011) Corros Sci 53:3156
31. Wang S, George K, Nesic S (2004) High pressure CO_2 corrosion electrochemistry and the effect of acetic acid. CORROSION/2004, Paper no. 375, NACE
32. Fajardo V, Canto C, Brown B, Young D, Nesic S (2008) The effect of acetic acid on the integrity of protective iron carbonate layers in CO_2 corrosion of mild steel. CORROSION/2008, Paper no. 333, NACE
33. Eliyan F, Alfantazi A Electrochemical corrosion evaluation of API-X100 pipeline steel in mildly alkaline, low oil bicarbonate emulsions. Corrosion (under review)
34. Gusmano G, Labella P, Montesperelli G, Privitera A, Tassinari S (2006) Corrosion 62:576